MSDE IChemE

Optimizing Linear Polymer Affinity Agent Properties for Surface-enhanced Raman Scattering Detection of Aflatoxin B1

Below are our statements about design, system, and application for this journal:

Polymer affinity agents serve as a robust and inexpensive capture agent for various targets of interests due to their non-specificity. Their repeat units serve as binding sites for targets and allow to potential for multiplex detection in various matrices. Herein, we have designed a series of polymer affinity agents with various chain lengths to capture aflatoxin B1: a well-studied and relevant target. Coupling these capture agents with surface-enhanced Raman scattering, isothermal titration calorimetry, and computational studies, we are able to predict and monitor binding between analyte and affinity agent. We actively show that the methodology involved in the order that we allow toxin and polymer to interact affects the sensor's overall performance. Anchoring chemistry also plays a significant role in the sensitivity of the sensor. This system's unique combination of analytical, polymer, and materials chemistry helps improve our understanding on how to engineer an inexpensive and versatile sensor.

Optimizing Linear Polymer Affinity Agent Properties for Surface-enhanced Raman Scattering Detection of Aflatoxin B1

Victoria M. Szlag[a†], Rebeca S. Rodriguez[a†], Seyoung Jung[b], Marc R. Bourgeois[c], Samuel Bryson[a], Anatolii Purchel[a], George C. Schatz[c], Christy L. Haynes[a], Theresa M. Reineke[a]

A series of poly(N-acryloyl glycinamide) (pNAGA) polymers were synthesized and studied as capture agents for surface-enhanced Raman scattering (SERS) detection of aflatoxin B1 (AFB1), a highly carcinogenic food-borne toxin. Four molecular weights of pNAGA were synthesized by reversible addition-fragmentation chain-transfer (RAFT) polymerization to study the dependence of affinity agent efficacy on chain length for this AFB1 sensing platform. Isothermal titration calorimetry (ITC) was used to verify the sign and magnitude of the enthalpic effects involved in polymer-AFB1 interactions in solution and to understand the effects of pNAGA chain length on AFB1 noncovalent binding. pNAGA-AFB1 interactions were found to be exothermic, and longer pNAGA chains generally resulted in smaller enthalpy decreases per repeat unit. With pNAGA$_{22}$ being thermodynamically the strongest affinity agent, we hypothesize that AFB1 affinity is determined by a balance between the configurational restrictions in pNAGA chains and the enthalpic advantage of binding AFB1. SERS spectral changes observed following AFB1 exposure were used to evaluate the influence of polymer molecular weight (2.0 – 5.2 kDa), order of attachment (pre- vs. post- functionalization of the substrate) and attachment chemistry (thiol vs. trithiocarbonate) on the sensitivity of AFB1 detection. The method by which target, polymer affinity agent, and signal transduction mechanism are combined was found to have significant impacts on the achieved sensitivity. The most effective polymer chain length (pNAGA$_{22}$), anchoring chemistry (thiol), and polymer/toxin assembly scheme (in-solution) allowed detection of 10 ppb AFB1 in water (below the FDA regulatory limit of 20 ppb), a hundred-fold improvement over SERS sensing without the pNAGA affinity agent.

Introduction

Polymer affinity agents have great potential to capture and detect important analyte targets; as such, they have been used for applications in food, medical, and water safety.[1] While literature precedent demonstrates that polymers can enable sensitive, inexpensive, and robust sensing devices, they are currently underutilized compared to more traditional affinity agents such as antibodies and aptamers. In the majority of published work, polymers are used as the matrix to immobilize more traditional sensing elements,[2-4] but given their benefits, such as facile synthesis, low cost, and ease of chemical modification, they can be used directly as affinity (analyte-capturing) agents.[5] Linear polymer analyte-capturing agents complex to their analyte freely in a matrix, while affinity agents like molecularly imprinted polymers (MIPs) completely immobilize the analyte in the matrix. MIPs play a hybrid role between acting as the matrix and as the affinity agent. MIPs are polymer affinity agents templated around a specific target and cross-linked to form a three-dimensional binding pocket[6,7] and have been well studied in sensor and analyte capture studies.

MIPs can be synthesized with desired analyte selectivity, using molecular hypotheses about target/polymer interactions.[8] While MIPs are well-studied as sensing elements that are robust and specific to target detection, they are often difficult to synthesize and characterize.[1] In addition, because they are cast to bind a particular target, they are not typically capable of detecting multiple targets at once. In contrast, in this work, we focus on the synthesis and optimization of linear polymer affinity agents that rely on chemical interactions between the polymer and target of interest with a long-term goal detecting multiple targets.

Linear polymer affinity agents enable the control of chain length, where each monomer repeat unit can serve as a binding site for a specific target of choice.[9,10,11] Control of affinity agent length also facilitates use of signal transduction mechanisms with small probe volumes such as total internal reflection fluorescence, attenuated total reflectance infrared absorption, or surface-enhanced Raman scattering. Interactions between polymer and target can range from use of specified binding pockets in protein targets to simple hydrogen binding and use of broader intermolecular interactions with small molecule targets.[12,13] When combined with techniques that can give a specific molecular signature such as SERS, less selective interactions present the possibility for multiplex detection where a single polymer affinity agent has the potential to facilitate detection of a multitude of targets.[14,15] Additionally, controlled polymerization allows the ability to tailor the end groups to facilitate attachment to the surfaces of either substrates or nanoparticles.[16,17] Exploiting the anchoring chemistry and the low-specificity interactions of a polymer affinity agent in combination with an analytical technique that

a. *Department of Chemistry, University of Minnesota, Minneapolis, Minnesota 55455, United States*
b. *Department of Chemical Engineering and Material Science, University of Minnesota, Minneapolis, Minnesota 55455, United States*
c. *Department of Chemistry and International Institute for Nanotechnology, Northwestern University, 2145 Sheridan Road, Evanston, Illinois 60208 United States*
† These authors contributed equally.
Corresponding Authors
*E-mail: chaynes@umn.edu Phone (work): 612-626-1096. Fax: 612-626-7541.
*Email: treineke@umn.edu Phone (work): 612-624-8042, Fax: 612-626-7541.
Electronic Supplementary Information (ESI) available: [details of any supplementary information available should be included here]. See DOI: 10.1039/x0xx00000x

gives the molecular fingerprint of a target represents an exciting and flexible sensing modality.

The popularity of surface-enhanced Raman scattering (SERS)[18–20] as a signal transduction mechanism stems from the analytical advantages of this technique: analyte-unique vibrational signatures, compatibility with aqueous matrices, and low limits of detection. The unique analyte signature produced[21] is due to the Raman scattering of light based on the vibrational modes of the analyte molecule. When an analyte is confined near a plasmonic metal surface, low concentrations of this analyte can be detected.[22] The surfaces displaying the needed localized surface plasmon resonance (LSPR), typically have nanoscale roughness which produces short range, intense electromagnetic (EM) fields[23] and leads to large Raman signal enhancement.[24] Consequently, many SERS detection platforms rely on affinity agents, such as polymers, to capture and concentrate analytes in this enhancing electromagnetic field that extends but a few-nanometers.

Although the use of linear, single-point-attachment polymers as SERS affinity agents has not been widely studied, previous work has demonstrated the utility of such a platform for sensing a protein toxin in food matrices.[25] In that work, the polymer affinity agent was designed with pendant saccharides to capture a protein biotoxin by exploiting a natural binding pocket present on the protein. Like protein toxins, small molecule biotoxins, such as those produced by algae in drinking water resources[26] and fungi that contaminate food,[27] require constant monitoring to ensure safety of ingestion and mitigate these serious threats to the general public.[28]

We have selected aflatoxin B1 (AFB1) as the sensing target for this work as this mycotoxin (produced by fungi) is the most toxic and carcinogenic variant, and as such, is heavily regulated world-wide (the US FDA regulatory limit for AFB1 in food is 20 ppb).[29][30] Other monitoring techniques for AFB1 have been used commercially, including enzyme linked immunosorbent assays

(ELISAs), monoclonal antibody affinity chromatography, lateral flow strips, fluorescence technology, and high performance liquid chromatography (HPLC).[36] Herein, we synthesize and explore the use of a new polymer affinity agent, *N*-acryloyl glycinamide (NAGA), to directly detect AFB1 via a SERS detection platform. We combine a well-characterized, simple, and inexpensive film over nanosphere (FON) wafer as our SERS substrate.[25,31–34] These FONs are fabricated via nanosphere lithography[35] and serve as an anchoring substrate for our polymer affinity agents. Previous work has shown that the successful SERS detection of aflatoxins can be based on the characteristic output of the target. This type of SERS detection could enable multiplex detection in the presence of other mycotoxins, theoretically without compromising sensitivity, specificity, or speed.

Inspired by the previous work by Piletska *et al.*, the NAGA repeat unit and polymerized variants were designed to function as the AFB1 binding site. We hypothesized that NAGA and AFB1 would noncovalently bind based on interactions similar to those reported between *N,N,*-methylene bisacrylamide (MBAA) and AFB1.[37] Through reversible addition-fragmentation chain transfer (RAFT) polymerization, both the function of NAGA was preserved (for AFB1 binding) and the polymer end groups tailored for binding to gold. We investigated how SERS detection of the analyte was affected by polymer chain length, endgroup (promotes covalent attachment to the SERS substrate), and the order of polymer chain addition to the detection platform: pre-functionalized to the gold surface prior to AFB1 exposure or post-functionalized to the gold surface after AFB1 exposure (Figure 1).

Overall, AFB1 sensing is an interesting and relevant system from which to explore the utility of polymer affinity agents for sensing platforms, and the impact of chain length, attachment chemistry, and order of affinity agent/target exposure on sensor performance.
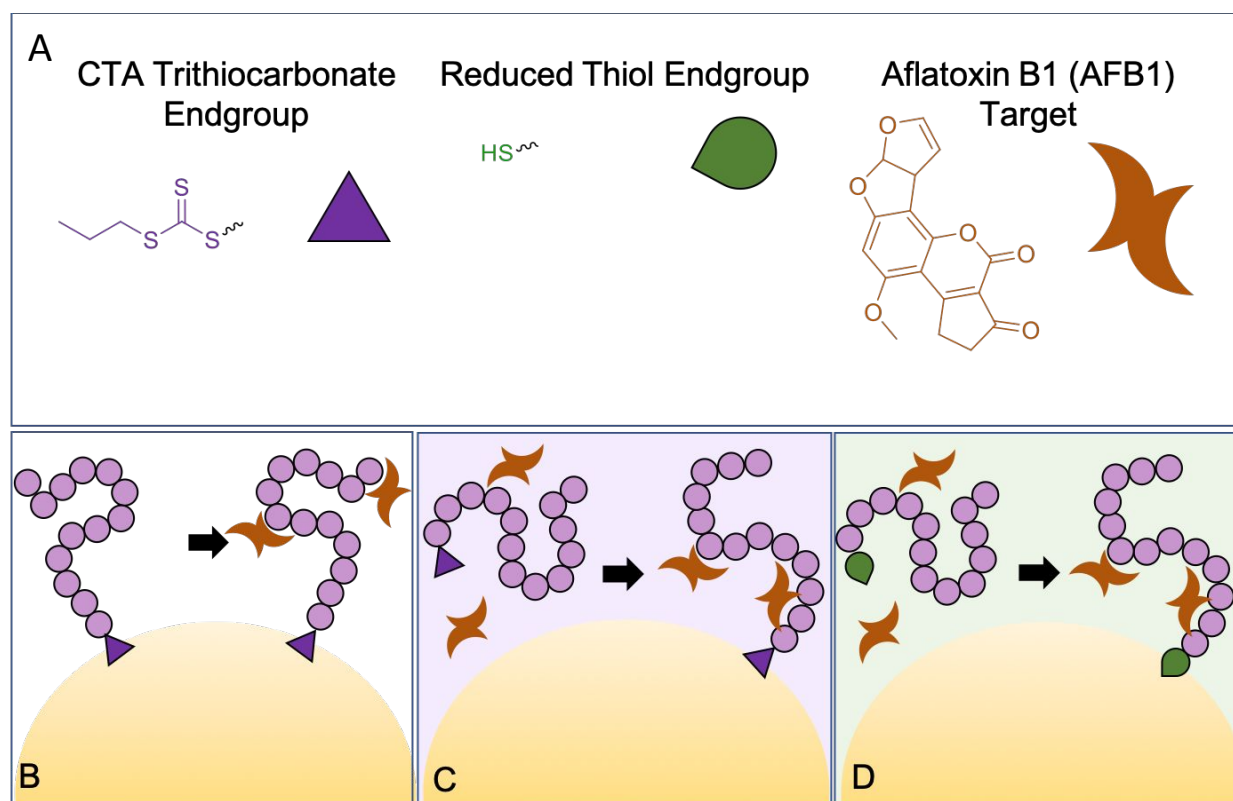
Figure 1. Illustrative representation of the studies explored in this work. A. Legend describing end groups (purple triangles: trithiocarbonate ends, green teardrop: thiol end group, and orange sickles: aflatoxin B1), B. traditional scheme of polymer (purple polymerized spheres) anchoring to gold FON surface (large yellow half-sphere) and subsequent AFB1 association, C. in-solution interactions of CTA-polymer and AFB1 before anchoring to gold FON surface, D. in-solution interactions of thiolated polymer and AFB1 before anchoring to gold surface.

Materials and Methods

Materials

Chemicals were used as purchased unless specified otherwise. Potassium carbonate, anhydrous (Certified ACS) was purchased from Fisher Chemical. Tris(2-carboxyethyl)phosphine hydrochloride (TCEP, ≥98%), N-propylamine (≥99%), glycinamide hydrochloride (≥98%), aflatoxin B1 from *Aspergillus flavus* (AFB1, ≥98%), and 4,4'-azobis(4-cyanovaleric acid) (V501, ≥75%), were purchased from Sigma-Aldrich. The chain transfer agent (CTA) 4-cyano-4-(propylsulfanylthiocarbonyl)sulfanylpentanoic acid (CPP) was synthesized as previously reported.[38] Silica spheres, 590-nm-diameter (10% solids), were purchased from Bangs Laboratories, Inc (Fishers, IN). High purity gold (99.999%) Au was purchased from Kurt J Lesker, (Clairton, PA).

Synthesis of *N*-acryloyl glycinamide (NAGA) Monomer

The monomer N-acryloyl glycinamide was prepared as previously reported by Seuring *et al*,[39] omitting the final purification step of recrystallization. Briefly, 4.59 g glycinamide hydrochloride (41.4 mmol) and 11.3 g potassium carbonate (81.3 mmol) were dissolved in 25 mL water and cooled in an ice bath. Under rapid stirring (300 rpm), 63.3 mL of 0.68 M acryloyl chloride in diethyl ether solution was added over 30 minutes. The flask was further stirred at room temperature for 2 hrs. Safety note: pressure can build in the reaction flask, and a venting mechanism is recommended. Removal of the diethyl ether, freeze drying of the aqueous layer, extraction of the crude solid with acetone, and purification of the crude extraction solution by column chromatography were performed as previously reported.[39] Yield of monomer after the column was 3.0 g (57%). DSC (rate of heating = 10 K/min; Figure S1): T_m = 137 °C. ^{1}H NMR (500 MHz, DMSO$_d$; Figure S2): δ = 3.73 (s, 2H, N-CH_2-$CONH_2$), 5.61 (dd, 1H, CH), 6.11 (dd, 1H, CH_2), 6.31 (dd, 1H, CH_2), 7.03 (s, 1H, NH_2), 7.36 (s, 1H, NH_2), 8.27 (s, 1H, NH).

Synthesis of poly(*N*-acryloyl glycinamide) (pNAGA) Polymers

The four molecular weights of pNAGA polymer were prepared by RAFT polymerization, similar to previously reported work. The polymerizations were performed in dimethyl sulfoxide (DMSO). For each synthesized molecular weight, molar concentrations and volumes of the monomer NAGA, initiator 4'-azobis(4-cyanovaleric acid), and chain transfer agent (CTA) 4-cyano-4-(propylsulfanylthiocarbonyl)

sulfanylpentanoic acid added can be found in Table S1 in the Supporting Information. A typical polymerization was carried out as follows: the monomer, initiator, and CTA were dissolved independently in DMSO, combined in the reaction flask and degassed by three cycles of freeze, pump, thaw. The reactions were then polymerized for 16 h at 75 °C. Polymer samples were dialyzed against 700 mL water for 18 h followed by two 700 mL water exchanges for 3 h each. The samples were lyophilized and characterized by size exclusion chromatography (SEC) and NMR. For SEC (Agilent 1260 Infinity Quaternary LC System with Eprogen columns at 40 °C [CATSEC1000 (7 μm, 50 × 4.6), CATSEC100 (5 μm, 250 × 4.6), CATSEC300 (5 μm, 250 × 4.6), and CATSEC1000 (7 μm, 250 × 4.6)]; Wyatt HELEOS II light scattering detector (λ = 662 nm) at 30 °C, and an Optilab T-rEX refractometer (λ = 658 nm)); 0.1 M Na_2SO_4 in 1.0 wt % acetic acid mobile phase; dn/dc = 0.185, traces can be seen Figure S3. ^{1}H NMR (500 MHz, $DMSO_d$; Figure S4): δ = 0.95 (s, 3H, -CH_3 end group), 1.24-2.07 (m, 3H, CH-CH_2 backbone), 3.57-4.05 (m, 2H, CH_2), 7.08-8.68 (m, 3H, NH & NH_2).

Reduction of pNAGA Trithiocarbonate End Groups to Thiols

Reduction of the end groups to thiols was carried out following a protocol by Zhou *et al*.[40] 0.06 g of $pNAGA_{22}$ was dissolved in 10 mL Mili-Q water (2.2 mM) and purged under nitrogen gas for 30 minutes. *N*-propylamine (2 mmol) and tris(2-carboxyethyl) phosphine HCl (TCEP) (0.04 mmol) were dissolved into the polymer solution and stirred overnight to ensure full conversion. Modification was confirmed via observation of SERS vibrational changes (see Figure S10 in Supporting Information) detailed in Results and Discussion.

Isothermal Titration Calorimetry (ITC)

ITC measurements of the pNAGA-AFB1 systems were performed using a MicroCal PEAQ-ITC Automated (Malvern Instruments, Westborough, MA) at 25 °C, similar to previously published work.[41] All solution transfers and injections were automated. Cleaning of the sample cell and injection syringe with subsequent 20% Contrad 70 detergent, water, and methanol preceded all titrations in this study. The instrument syringe was flushed with 10% bleach after experiments. Polymer solutions were made at a concentration of 4.0 mM NAGA repeat units in 22 vol% DMSO, 16 vol% methanol, 62 vol% acetate buffer (pH 5) and transferred to the injection syringe. The DMSO/MeOH/acetate buffer mixture was used to create 0.26 mM AFB1 solutions, or as a blank solvent for background titrations, and was transferred to the sample cell. The titrations consisted of 1.5 μL injections of pNAGA solution (in syringe) into AFB1 solution or blank solvent (in sample cell) every 150 s. Raw ITC data (as seen in the left two columns of Figure S5) are measured as heat flow rate as a function of time, displaying a peak with each injection. Final ITC results, depicting total heat absorption at each injection versus polymer repeat unit (RU)/toxin ratio, are the integration of the raw heat flow data with respect to time. The enthalpy change exclusively from AFB1-polymer interactions (ΔH_{int}) was determined by subtracting (point-by-point) the enthalpy change measured in

the background titration of polymer injected into solvent (ΔH_{bgd}) from that in the main titration of polymer injected into AFB1 (ΔH_{main}).

Surface-enhanced Raman Scattering (SERS)

SERS measurements were performed using a Snowy Range Instruments SnRI ORS system with 785 nm laser, 9 mW incident power, and 10 sec integration time. The SERS substrates used, gold film over nanospheres (FON) with a localized surface plasmon resonance maximum between 720-820 nm as measured by a fiber optic probe (Ocean Optics, Dunedin, Florida) with a flat gold film as the reflective standard, were fabricated as previously reported.[25,32,41] Non-resonant Raman spectra of the monomer NAGA under 785 nm excitation were calculated with the Amsterdam Density Functional (ADF) computational chemistry package[42], using Becke-Perdew (BP86)[43] generalized gradient approximation (GGA), and B3LYP[44] hybrid exchange-correlation functionals, as previously reported.[41]

In this work, two types of SERS experiments were conducted: post-polymer attachment AFB1 exposure and pre-polymer attachment AFB1 exposure. In the former, pNAGA was first attached to the gold FON by incubating the FON in a 1.0 mM pNAGA solution for 18 h. Subsequently, the pNAGA-functionalized FONs were exposed to a known concentration of AFB1 dissolved in 4:6 MeOH/water for 6 h. The FONs were rinsed with 1 mL of water, dried, and measured by SERS.

In the pre-polymer attachment AFB1 exposure, a 1.0 mM pNAGA solution was incubated with a known concentration of AFB1 dissolved in 4:6 MeOH/water for 6 h. Bare FONs were then exposed to the pNAGA/AFB1 solution for 18 h, rinsed with 1 mL of water, air dried, and measured by SERS. SERS spectra were measured on 5 spots per FON, and three FON replicates were performed per experiment. The five SERS spectra from each FON were averaged, baselined (Origin 9.1, eleven anchor points, found using the first and second derivative with Savitzky-Golay smoothing, and connected by B-spline interpolation, utilizing the same number of points as the input spectrum), and normalized by the incident power and integration time. Statistical analysis of FON intensities was evaluated and accounted for. Peak height and ratios that appeared to be AFB1 concentration-dependent were statistically analyzed by one-way ANOVA with a Tukey post-hoc analysis using the program R.[45]

Results and Discussion

AFB1 on Bare FONs

SERS of AFB1 without affinity agents either has sufficient LODs (13-36 ppb) but poor reproducibility due to substrate problems[46] or excellent reproducibility at LODs (15 ppm) above the regulatory limit.[47] AFB1 SERS sensors that have used affinity agents have focused on either aptamers (LOD 0.03 ppb AFB1)[48] or antibodies (LOD 0.10 ppb).[49] However, both examples are extrinsic SERS sensors, which does not measure the vibrational modes of the target directly, but instead monitors a SERS

reporter. Such extrinsic sensing loses the benefit of SERS as a label-free technique, inherently capable of multiplex detection based on specific vibrational modes of AFB1 and other analytes. Therefore, to enable a generalizable platform that has potential for multiplex detection via intrinsic SERS signals, the efficacy of polymer affinity agents must be tested for small molecule analytes like AFB1.

AFB1 can associate directly with the gold FON surface through delocalized pi interactions, thus, bare FONs were exposed to AFB1 solutions as a control experiment. A peak at

936 cm^{-1} shift was observed, growing in with increasing AFB1 concentration, whereas a shoulder of the 995 cm^{-1} shift peak indicated adventitious species adsorbed on the bare FON in Figure 2. A previous AFB1 SERS experiment on silver substrates has reported a ring breathing/C-O stretch at 934 cm^{-1} shift.[47] Normalizing the AFB1 peak to the native FON peak, the measured signal was significantly different from the 0 ppm at 1 ppm. Because the regulated limit of AFB1 by the FDA is well below 1 ppm, at 20 ppb, this provides sufficient motivation for the use of an affinity agent to detect AFB1 with SERS.
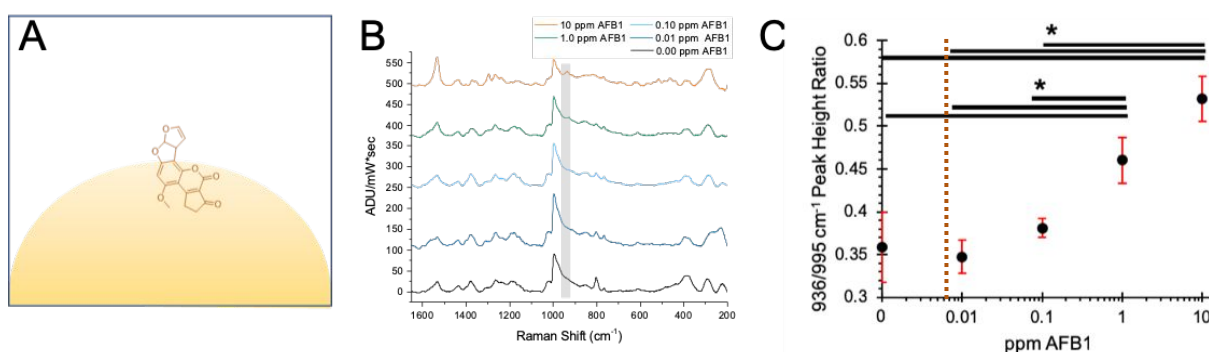
Figure 2. SERS from AFB1 on bare FONS; (A) cartoon representation, (B) spectra from FONs exposed to 0.01-10 ppm AFB1, (C) the average 936 cm^{-1} shift height normalized by 995 cm^{-1} shift; error bars represent standard deviation and * denotes $p < 0.05$. Dotted line indicates FDA limit (20 ppb).

Synthesis of pNAGA Polymers for AFB1 Binding
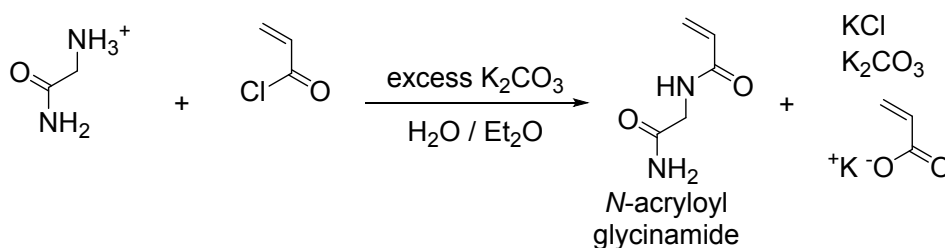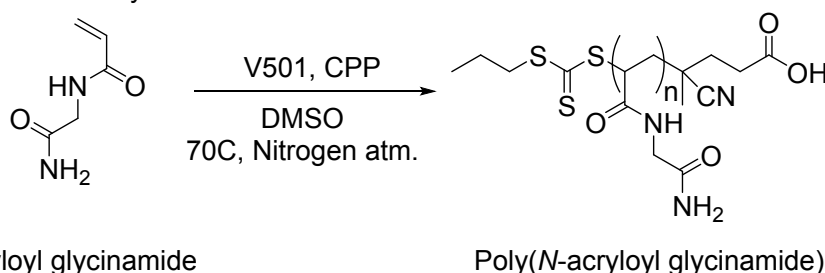
Scheme 1. (A) NAGA synthesis (B) RAFT polymerization of NAGA

For this study, four polymer lengths were synthesized by RAFT polymerization to enable the systematic study of chain length on affinity agent performance. It was hypothesized that a mid-range molecular weight of pNAGA would perform best by maximizing the number of binding sites (repeat units) without being so large as to coil and form competing intramolecular H-bonds, as previously seen with other long-chain polymers binding AFB1 in solution.[41]

Synthesis of the NAGA monomer followed a procedure that minimized acrylic acid impurities, a common side product in the reaction of acryloyl chloride and glycinamide hydrochloride, due to the importance of the presence of pendent amide for interaction with the biological toxin AFB1. These byproducts cannot be observed by NMR (Figure S2 in Supporting Information) and must be detected at <1% wt by DSC. The T_m of the synthesized monomer is 136 °C

(Figure S1 in Supporting Information) and is lower than that reported for ultrapure NAGA samples (143 °C, <0.01 % acrylate) but higher than reported samples with 0.12% acrylic acid (132 °C), indicating an acrylic acid content <0.12%.[39] Because only the thermal properties are disrupted by such low amounts of acrylic acid (not the focus of this work) our analysis indicated that the NAGA monomer was sufficiently pure for polymerization. The polymers synthesized did not exhibit UCST behavior, likely due to the acrylic acid impurity. Using the chain transfer agent (CTA) 4-cyano-4-(propylsulfanylthiocarbonyl)sulfanylpentanoic acid (CPP), four molecular weights of pNAGA were polymerized by RAFT (Table 1). In addition to providing useful sulfur moieties for later gold attachment,[50–52] the use of RAFT polymerizations resulted in low dispersities, which enable the study of size-dependent effects within the polymer series. The targeted chain lengths spanned from oligomeric to moderately sized polymers to enable the study of chain length-dependent trends in AFB1 interactions, exposed either in solution or on the gold SERS substrates. Based on previous work with amine and alcohol pendent polymers[41], it was hypothesized that short-mid chain lengths would demonstrate higher affinity per repeat unit in solution due to low intramolecular interactions and low chain coiling, molecular behaviors which result in higher availability of binding to each repeat unit.

Table 1. Characterization of pNAGA polymers synthesized by RAFT, number of NAGA repeat units are denoted in name subscript; M_n, M_w, and Đ measured by SEC.

Polymer	M_n (kDa)	M_w (kDa)	Đ
pNAGA$_{38}$	5.11	5.52	1.08
pNAGA$_{30}$	4.08	4.53	1.12
pNAGA$_{22}$	3.12	3.40	1.09
pNAGA$_{14}$	2.01	2.25	1.12

In-Solution Interactions of pNAGA with AFB1

The in-solution interaction of pNAGA and AFB1 was studied by measuring the enthalpy change in the system when pNAGA was titrated into a solution of AFB1, using ITC. ITC has long been used to quantify protein/ligand interactions, and has more recently been used to study polymer systems, such as the interactions between polycations and DNA.[53] In our system, we controlled the concentration of repeat units, which are the hypothesized AFB1 binding sites, to be the same for each polymer solution. If enhanced binding effects were observed due to more binding sites localized to a single chain (i.e. longer chains), the enthalpy change per repeat unit would be greater at a given RU/toxin ratio, compared that with a shorter chain.

Dilute, buffered pNAGA solution ([RU] = 4.0 mM) was titrated into AFB1 solution (0.26 mM) prepared with the same solvent mixture, and heat release was observed for all polymers (Figure S5 in Supporting Information). Note that heat was released during polymer dilution (into blank solvent) to a much smaller extent. Subtracting ΔH_{bgd} from ΔH_{main}, it was found that pNAGA-AFB1 interactions are exothermic, indicating enthalpically favorable

noncovalent interactions between pNAGA and AFB1,[54] as expected from the simulations of a similar bisamide binding AFB1.[37]

The instantaneous enthalpy change as a function of RU/toxin molar ratio was plotted and compared between different chain lengths of pNAGA. Figure 3 compares the integrated, background-subtracted data. The absence of the classic sigmoidal shape precludes the typical binding model-based fitting of the data; however, important trends within the pNAGA series are still apparent. The shorter chain lengths of pNAGA$_{14}$ and pNAGA$_{22}$ showed larger magnitudes of binding enthalpy per repeat unit than their longer counterparts, pNAGA$_{30}$ and pNAGA$_{38}$. This is suspected to be due to entropic restrictions in pNAGA chain conformation and potential intramolecular interactions, which may decrease the effective number of available "binding sites." A similar trend has previously been observed with comparable chain lengths of poly(2-hydroxyethyl methacrylate) (pHEMA) where consideration of the ITC conditions for AFB1 and polymers is further discussed and optimized.[41]
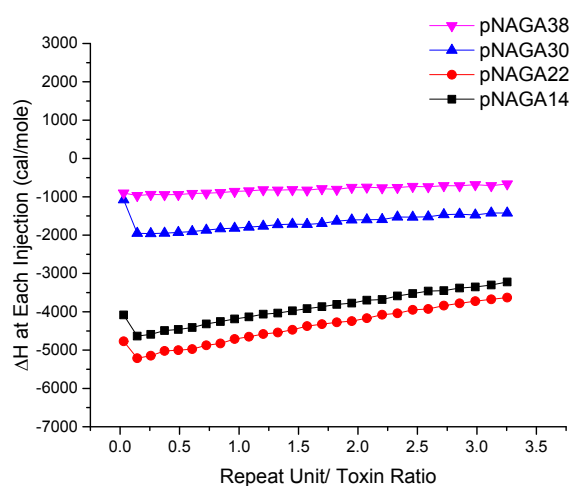
Figure 3. Integrated ITC profiles of pNAGA polymers (4.0 mM RU) titrated into 0.26 mM AFB1. All titrations were performed in 22% DMSO, 16% methanol, 62% acetate buffer (pH 5).

Computational Modeling of Monomer To assist with the interpretation of experimental SERS spectra from pNAGA, the non-resonant Raman scattering spectrum of the monomer N-methacryloyl glycinamide (NMAGA) was calculated using density functional theory. The calculated spectrum is used to rationalize the measured Raman frequencies and attribute them to specific vibrational modes within the molecule. Figure 4 shows the calculated spectrum of NMAGA plotted with a previously reported calculated spectrum of dipropyl carbonotrithioate (DPCTT), to represent the signal from the CPP anchor group. A full list of peak assignments can be found in the Supporting Information (Table S2). Using this information, we identified peaks originating from vibrations of the primary amide: 611, 822, 1044, 1248, 1322, 1344, and 1561 cm^{-1} shift. It was hypothesized that some, or all, of these vibrations may experience frequency shifts or changes in relative amplitude as pNAGA associates with AFB1 via hydrogen bonding. Vibrational modes from the CPP anchor group were not anticipated to change

with AFB1 exposure. Strong vibrational modes from the anchoring group that did not overlap with modes from NMAGA, such as 516, 653, 959 and 1282 cm^{-1} shift, were proposed as appropriate groups for spectral normalization.
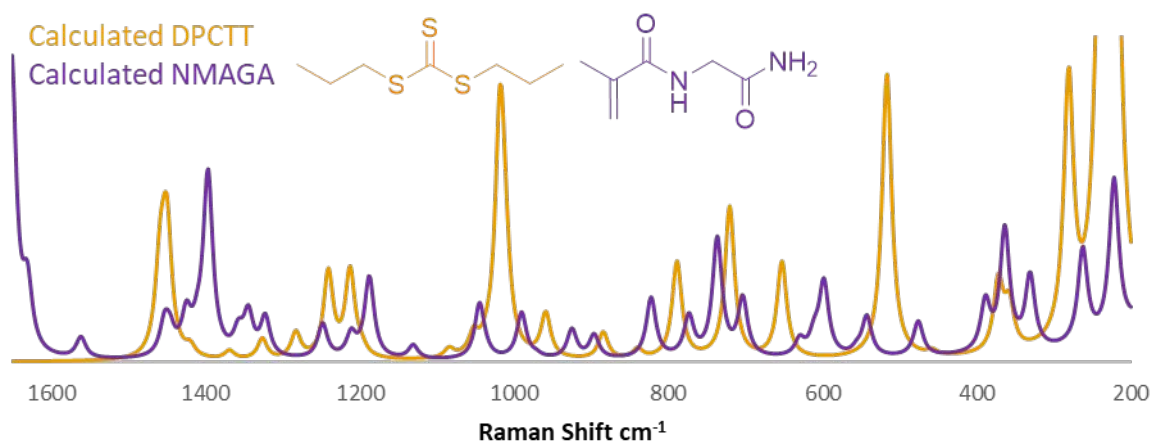
Figure 4. Calculated normal Raman spectrum of NMAGA plotted with calculated normal spectrum of DPCTT as shown by our previous work.[41]

In addition to enabling predictions about spectral changes due to AFB1, the calculated normal Raman spectra assisted in the characterization of the polymer on the SERS substrate. Proximity and orientation of an affinity agent on a SERS surface can change the magnitude, and to a lesser extent, location of the vibrational bands, when comparing computed spectra to experimental spectra. Significant broadening of the pNAGA experimental spectra was observed relative to the computed monomer spectra as expected due to the spectral averaging of the ensemble of real chain conformational changes relative to the SERS substrate. All four molecular weights of pNAGA demonstrated a pattern of vibration similar to those predicted (Figure S6). The SERS of the four polymers gave further chemical information. With increasing chain length, relative peak magnitudes changed for several pNAGA and CPP vibrations, shown in the shaded regions of Figure S6 in the Supporting Information.

Table 2 compares our experimental spectra to our computed spectra. Vibrational bands assigned to the monomer and CTA structure were labeled and used to monitor changes in intensity as chain length increases. Because an increase in repeat unit character can be observed across the four pNAGA polymers, we can conclude that the longest chain length of pNAGA grafted to the surface has more repeat units within the probe volume of our SERS substrate than the immediately shorter pNAGA polymer. Thus, all polymers were determined to be valid, candidate affinity agents for AFB1 detection by SERS; all possessed multiple AFB1 interactions sites that were within the enhancing electromagnetic field. SERS spectra of each polymer chain length anchored to the SERS surface can be seen in the SI (Figure S6). Polymer and CTA vibrations change based on increasing chain length. Based on both ITC and SERS results, pNAGA$_{22}$ was used to evaluate the optimal AFB1 complexing scheme and polymer anchor chemistry.

Table 2. A comparison of polymer experimental spectra to computed monomer and CTA spectra. An increase or decrease of peak maxima in the experimental spectra after FON attachment is denoted relative to computational monomer and CTA calculations. For atomic labels of monomer refer to Figure S5.

Experimental Vibrational Shift (cm^{-1})	Computed Monomer	Computed DPCTT (CPP)[41]
849	Increase in 822 cm^{-1} shift: (m) C5-C6 stretching, wagging of H's on N2, C4-N1-C5 bending	Increase relative to polymer in 884 cm^{-1} shift: C1-C2 and C2-C3 symmetric stretch, some wagging of H's on these C's
1199	1187 cm^{-1} shift: (m) C4-N1-C5 asymmetric stretch, twisting of C5 H's	Decrease relative to polymer in 1240 cm^{-1} shift: wagging of H's on C5 and C6, asymmetric stretch of S3-C5 and C5-C6 and 1282 cm^{-1} shift: in-phase twisting of H's on C1, C2, and C3
1377	Increase of 1397 cm^{-1} shift: (s) bending of H's on C3 and C1, coupled bending of angle between C1-C2-C4 with C2-C3 stretch	Increase relative to polymer in 1450 cm^{-1} shift: symmetric bending of H's on C1 and C2

AFB1 Sensing with pNAGA$_{22}$/AFB1 Complex

Traditionally, affinity agents are anchored onto surfaces and then exposed to a target for binding. It is fairly common to anchor molecules onto SERS substrates via sulfur-based chemistry, and many researchers have reported this with alkanethiol chains, MIPs, and thiolated ligands on gold nanoparticles.[55,56,57] While this attachment scheme has been successful in other work, we hypothesized that a surface-bound polymer lacks sufficient conformational mobility to enable optimal target binding. For this reason, we employed a less traditional route to sense AFB1 with our polymer affinity agents. While in solution, a polymer is able to move more freely, exposing more of the polymer's repeat units, allowing optimal conformation to noncovalently bind the maximum number for AFB1 molecules. In this pre-attachment exposure, we allow AFB1 to interact with the free polymer in solution and then attach the bound, complexed molecules onto the SERS substrate (Figure 6A). Spectra of post-attachment exposure can be seen in the SI (Figure S7).

Increasing AFB1 concentrations complexed with pNAGA$_{22}$ showed spectral changes relative to 0 ppm control experiment (Figure 6B). The two spectral changes that can be seen in all concentrations tested (as low as 10 ppb) was the increasing ratio of 1242 cm^{-1} shift band relative to the 1195 and 1279 cm^{-1} shift bands, and the increased magnitude at 1381 cm^{-1} shift. As previously stated, both the primary amide on pNAGA (1242 and 1377 cm^{-1} shift) and AFB1 (1249 and 1355 cm^{-1} shift), the proposed hydrogen bonding partners in the affinity agent/target complex, have strong modes in these regions.

The spectral change most dependent on AFB1 concentration was found to be the peak height at 1381 cm^{-1} shift, normalized by the CPP vibration at 688 cm^{-1} shift (identified above from the calculated spectrum). Using a one-way ANOVA and Tukey post hoc analysis, this peak change was statistically significant as low at 100 ppb. This spectral feature, observed in the averages as low 10 ppb, was not significant at this lower concentration due to the high amount of variance between replicates. The source of this variance is believed to result from structural heterogenicity in the FON SERS substrates, which results in variance in the electromagnetic field, and thus spectra. Other peaks ratios were analyzed and were not statistically significant from one another. These results are an improvement to the convention of anchoring the affinity agent onto the substrate and then exposing it to the target of choice. LODs decrease from 50 ppm in the traditional method (Figure S7), to 100 ppb in this new method.
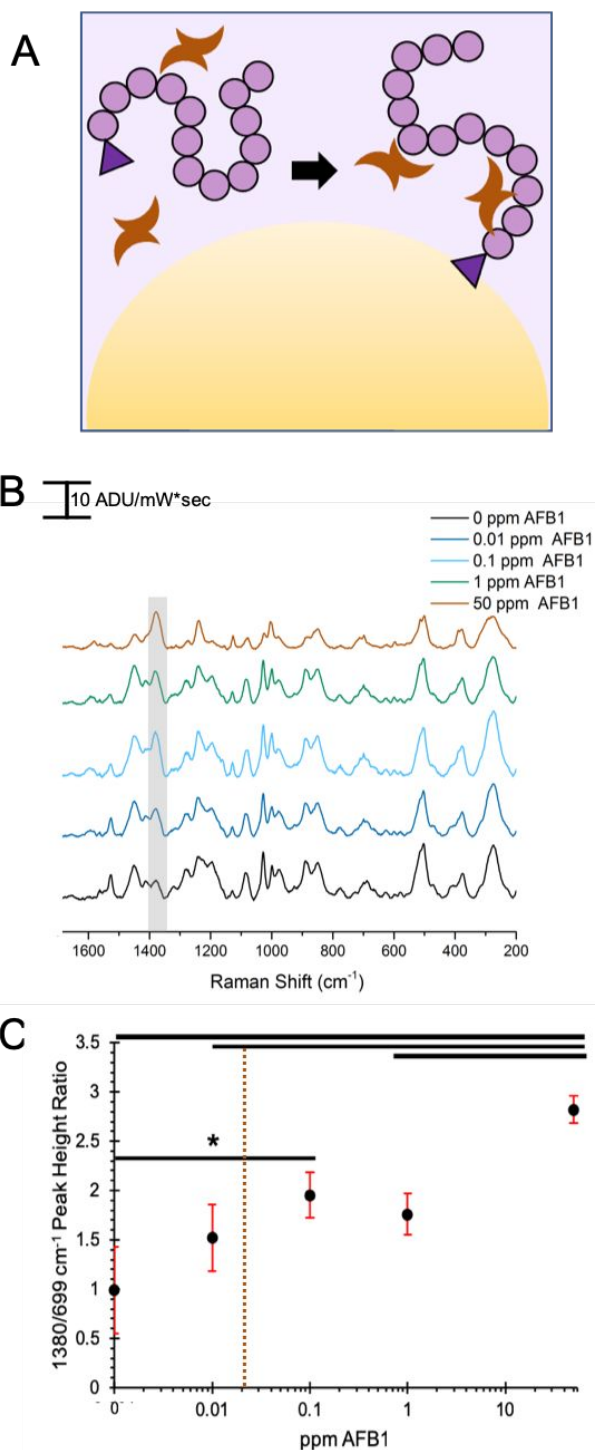
Figure 6. SERS from pNAGA$_{22}$/AFB1 complex assembled before immobilization on the SERS substrate; (A) schematic representation of the new exposure method (pre-exposure of the polymer containing a trithiocarbonate end group to AFB1 in solution and then tethering to the gold), (B) spectra of the complex form from 0.01-50 ppm, and (C) the average 1380 cm^{-1} shift peak intensity normalized by the 688 cm^{-1} shift peak intensity, the negative control (0 ppm) has been added to this plot as a point of reference; error bars represent standard deviation, and * denotes statistically significant differences (p< 0.05). Dotted line indicates FDA limit (20 ppb).

Reduction of the pNAGA Trithiocarbonate End Group

The RAFT chain transfer agent (CTA), in addition to controlling the radical polymerization, provides a functional handle shown to bind to gold surfaces important to SERS substrates.[50–52,58] This trithiocarbonate end group can be used to directly functionalize gold SERS substrates with the polymer or be reduced to a thiol, which also has a high affinity for gold surfaces.[40] We hypothesized that the thiol-terminated polymer would perform better than the trithiocarbonate-terminated polymer due to the smaller binding footprint, which could yield a higher density of affinity agents on the sensor surface, and offers fewer intrinsic S-C Raman vibrations that could mask AFB1 vibrational modes.

SERS detection of AFB1, enabled by in-solution interaction with pNAGA$_{22}$, relies on tracking spectral regions that include vibrations from the trithiocarbonate moiety of the pNAGA CTA group, the NAGA repeat units, and AFB1. Specifically, pNAGA$_{22}$ demonstrates strong trithiocarbonate vibrations at 1451 cm^{-1} shift (CH$_3$-CH$_2$ H bending), 1242 cm^{-1} shift (C=S and CH$_2$-CH$_2$ asymmetric stretch), 1195 cm^{-1} shift (CH$_3$-CH$_2$-CH$_2$ H rocking/twisting), 1028 cm^{-1} shift (C=S and C-C symmetric stretch), 888 cm^{-1} shift (CH$_3$-CH$_2$-CH$_2$ C-C symmetric stretch), 688 cm^{-1} shift (S-C stretch), and 503 cm^{-1} shift (symmetric 'breathing' of CS$_2$=S bonds). Our computational assignments of C=S vibrations are confirmed by precedent in the literature, where a strong C=S stretching mode can be observed anywhere from 1020 – 1250 cm^{-1}.[59,60] Thus, modifying this end group to a thiol was undertaken to decrease the number of pNAGA vibrational modes and potentially increase AFB1 signal masked by CTA-specific vibrational bands.

Using *N*-propylamine and tris(2-carboxyethyl) phosphine HCl (TCEP), the trithiocarbonate end group was reduced to a thiol group. With thiol endgroups, some coupling between the reactive thiols, resulting in disulfide species, is expected.[61] Disulfide coupled chains have been previously reported to bind more strongly to gold surfaces than polymers with a terminal sulfur moiety, an effect that is hypothesized to originate from cleavage of the S-S bond at the gold surface to yield a S–Au bond.[52] Modification of the end group was characterized by comparison of the pNAGA$_{22}$ SERS before and after reduction (Figure 7) and SERS of CTA-only before and after reduction can be seen in the Supporting Information (Figure S10). Decreased magnitude at CTA vibrations detailed above (1451, 1242, 1195, 1028, 888, 688, and 503 cm^{-1} shift) were observed, resulting in a pNAGA$_{22}$-SH spectrum with fewer peaks.
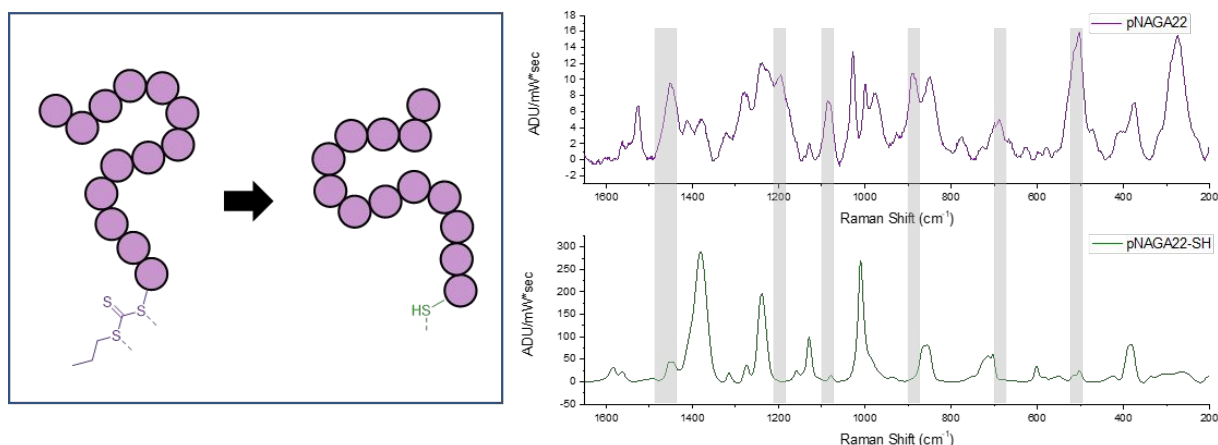
Figure 7. SERS characterizing the reduction of the trithiocarbonate to a thiol. Experimental details of this reaction can be seen in the SI.

AFB1 Sensing with pNAGA$_{22}$-SH/AFB1 Complex

Following the reduction of the polymer, pNAGA$_{22}$-SH was complexed with varying concentrations of AFB1 and then grafted onto the FON surface (Figure 8A). The SERS, normalized to the 702 cm^{-1} shift peak height, can be seen in Figure 8B. Fewer spectral changes due to AFB1 were identified using this method. The most notable feature was a growing shoulder at 712 cm^{-1} shift. The nearest assigned modes from pNAGA and AFB1 are a CH-C symmetric stretch, with small contributions from NH-CH$_2$-C bending, calculated at 736 cm^{-1} shift and C-H in-plane bending seen experimentally for AFB1 at 686 cm^{-1} shift,[47] respectively. Because these NAGA and AFB1 vibrations are not near the observed peak shift, we hypothesize the change seen at 702 cm^{-1} shift is due to a change in the S-C stretch of the thiol upon AFB1 complexation. In all concentrations tested (0.01, 0.1, 1, 10, and 50 ppm), the 712/702 cm^{-1} shift ratio was statistically different from the AFB1-free solvent control.

Most notably, complexing pNAGA$_{22}$-SH and AFB1 prior to SERS detection led to the lowest statistical discernment of AFB1 from the control (10 ppb). The US FDA regulatory limit for AFB1 is 20 ppb; this result clearly demonstrates the potential of our platform for relevant AFB1 detection. Yet, the platform did not provide multiple unique, assignable vibrations of AFB1, a desired feature for a SERS sensor that would be used to detect multiple analytes from complex samples. The degree of pNAGA$_{22}$-SH character in the spectra and weaker binding in solution are potential reasons for the lack of multiple spectral features. If pNAGA$_{22}$-SH exists as coupled disulfide chains in solution, based on the ITC results detailed above, we predict the coupled chains would have poor in-solution AFB1 binding due to an effective chain length of 44 repeat units. We have also performed these experiments using the traditional method, post-attachment exposure, and have outlined these in our Supporting Information

(Figure S7-S8). These spectra do not show significant signal at low concentrations of AFB1.
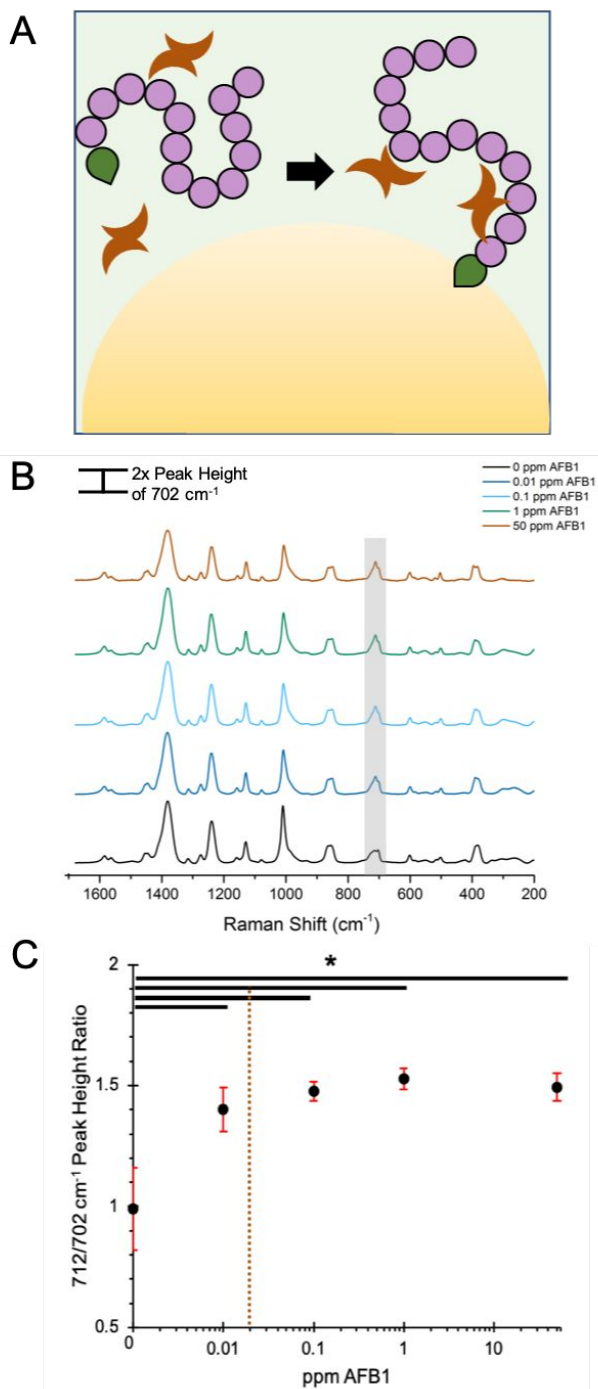
Figure 1. SERS from pNAGA22-SH/AFB1 complex assembled ahead of immobilization on the SERS substrate; (A) schematic representation of the exposure method (pre-exposure of the polymer containing the thiol end group to AFB1 and then tethering to the gold), (B) 702 cm^{-1} shift normalized spectra of the complex form from 0.01-50 ppm, (C) the average 712 cm^{-1} shift height normalized by 702 cm^{-1} shift, the negative control (0 ppm) has been added to this plot as a point of reference; error bars represent standard deviation and * denote statistical significance (p<0.05). Dotted line indicates FDA limit (20 ppb).

Conclusions

Herein, we explored polymer features that can be used to optimize their performance as affinity agents in sensing platforms. Starting from a monomer (NAGA) with hypothesized affinity for the biotoxin AFB1, and targeting SERS as a signal transduction mechanism, four polymers with distinct molecular weights were created by RAFT. These polymers were used to explore the role of molecular weight, anchoring chemistry, and order of addition (pre- or post- functionalization of the substrate) on the sensitivity of AFB1 detection. From our results, we posit three means by which polymer properties can influence performance as an affinity agent on a sensing platform: (1) In-solution, noncovalent binding between polymer and target is a function of the polymer chain conformation due to a decreased number of available binding sites on polymers engaged in intramolecular interactions; our ITC results demonstrated that shorter pNAGA polymers such as pNAGA$_{14}$ and pNAGA$_{22}$ performed better in solution than their longer counterparts, pNAGA$_{30}$ and pNAGA$_{38}$. (2) The untethered polymer in-solution enables improved target binding; complexing pNAGA$_{22}$ and AFB1 prior to SERS substrate attachment improved the detection limit of the polymer-SERS platform; the pNAGA$_{22}$/AFB1 complex was statistically different from the control at 100 ppb AFB1. (3) Altering the polymer attachment chemistry to decrease interference with the transduction mechanism of the sensor can significantly improve platform sensitivity; reduction of the trithiocarbonate to a thiol simplified the pNAGA$_{22}$-SH spesynthetsizctrum and complexing AFB1 and pNAGA$_{22}$-SH prior to SERS substrate attachment enabled detection of 10 ppb AFB1. The lowest concentration of AFB1 detected by the pNAGA-SH enabled SERS platform is below the US FDA regulatory limit of 20 ppb. Our thorough study of how molecular weight and anchoring chemistry affect AFB1 capture, and SERS detection, can inform the design of future sensing platforms targeting other analyte species. Based on our results, future work to detect AFB1 should use a pNAGA-SH <11 repeat units to have excellent in-solution capture of AFB1, and a simplified, lower magnitude pNAGA-SH signal that should enable the detection of multiple unique, assignable vibrations of AFB1. Such a platform would enable detection and differentiation of multiple analytes and, thus, make a commercially viable platform.

Conflicts of interest

The manuscript was written through contributions of all authors. All authors have given approval to the final version of the manuscript. The authors declare no competing financial interest.

Acknowledgements

Notes and references

1   (1) Vasapollo, G.; Sole, R. D.; Mergola, L.; Lazzoi, M. R.; Scardino, A.; Scorrano, S.; Mele, G. Molecularly Imprinted Polymers: Present and Future Prospective. *Int J Mol Sci* **2011**, *12* (9), 5908–5945. https://doi.org/10.3390/ijms12095908.

2   (2) Carvalho, W. S. P.; Wei, M.; Ikpo, N.; Gao, Y.; Serpe, M. J. Polymer-Based Technologies for Sensing Applications. *Anal. Chem.* **2018**, *90* (1), 459–479. https://doi.org/10.1021/acs.analchem.7b04751.

3   (3) Hydrogels in Sensing Applications. *Progress in Polymer Science* **2012**, *37* (12), 1678–1719. https://doi.org/10.1016/j.progpolymsci.2012.09.001.

4   (4) Electrochemical Sensors and Biosensors Based on Redox Polymer/Carbon Nanotube Modified Electrodes: A Review. *Analytica Chimica Acta* **2015**, *881*, 1–23. https://doi.org/10.1016/j.aca.2015.02.059.

5   (5) Molecularly-Imprinted Polymer Sensors: Realising Their Potential. *Biosensors and Bioelectronics* **2016**, *76*, 131–144. https://doi.org/10.1016/j.bios.2015.07.013.

6   (6) BelBruno, J. J. Molecularly Imprinted Polymers. *Chem. Rev.* **2018**. https://doi.org/10.1021/acs.chemrev.8b00171.

7   (7) Culver, H. R.; Peppas, N. A. Protein-Imprinted Polymers: The Shape of Things to Come? *Chem. Mater.* **2017**, *29* (14), 5753–5761. https://doi.org/10.1021/acs.chemmater.7b01936.

8   (8) Ting, J. M.; Tale, S.; Purchel, A. A.; Jones, S. D.; Widanapathirana, L.; Tolstyka, Z. P.; Guo, L.; Guillaudeu, S. J.; Bates, F. S.; Reineke, T. M. High-Throughput Excipient Discovery Enables Oral Delivery of Poorly Soluble Pharmaceuticals. *ACS Cent. Sci.* **2016**, *2* (10), 748–755. https://doi.org/10.1021/acscentsci.6b00268.

9   (9) Szlag, V. M.; Rodriguez, R. S.; He, J.; Hudson-Smith, N.; Kang, H.; Le, N.; Reineke, T. M.; Haynes, C. L. Molecular Affinity Agents for Intrinsic Surface-Enhanced Raman Scattering (SERS) Sensors. *ACS Appl. Mater. Interfaces* **2018**, *10* (38), 31825–31844. https://doi.org/10.1021/acsami.8b10303.

10 (10) Dahlström, M.; Jonsson, P. R.; Lausmaa, J.; Arnebrant, T.; Sjögren, M.; Holmberg, K.; Mårtensson, L. G. E.; Elwing, H. Impact of Polymer Surface Affinity of Novel Antifouling Agents. *Biotechnology and Bioengineering* **2004**, *86* (1), 1–8. https://doi.org/10.1002/bit.10900.

11 (11) Lee, J.; Sohn, J. W.; Zhang, Y.; Leong, K. W.; Pisetsky, D.; Sullenger, B. A. Nucleic Acid-Binding Polymers as Anti-Inflammatory Agents. *PNAS* **2011**, *108* (34), 14055–14060. https://doi.org/10.1073/pnas.1105777108.

12 (12) Hoffman, A. S. Bioconjugates of Intelligent Polymers and Recognition Proteins for Use in Diagnostics and Affinity Separations. *Clinical Chemistry* **2000**, *46* (9), 1478–1486.

13 (13) Chou, B.; Mirau, P.; Jiang, T.; Wang, S.-W.; Shea, K. J. Tuning Hydrophobicity in Abiotic Affinity Reagents: Polymer Hydrogel Affinity Reagents for Molecules with Lipid-like Domains. *Biomacromolecules* **2016**, *17* (5), 1860–1868. https://doi.org/10.1021/acs.biomac.6b00296.

14 (14) Mueller, M.; Tebbe, M.; Andreeva, D. V.; Karg, M.; Alvarez Puebla, R. A.; Pazos Perez, N.; Fery, A. Large-Area Organization of PNIPAM-Coated Nanostars as SERS Platforms for Polycyclic Aromatic Hydrocarbons Sensing in Gas Phase.

Langmuir **2012**, *28* (24), 9168–9173. https://doi.org/10.1021/la300454q.

15 (15) Vo-Dinh, T.; Stokes, D. L. Surface-Enhanced Raman Detection of Chemical Vapors with the Use of Personal Dosimeters. *Field Analyt. Chem. Technol.* **1999**, *3* (6), 346–356. https://doi.org/10.1002/(SICI)1520-6521(1999)3:6<346::AID-FACT4>3.0.CO;2-Q.

16 (16) Perrier, S. 50th Anniversary Perspective: RAFT Polymerization—A User Guide. *Macromolecules* **2017**, *50* (19), 7433–7447. https://doi.org/10.1021/acs.macromol.7b00767.

17 (17) Mathias, F.; Tahir, M. N.; Tremel, W.; Zentel, R. Functionalization of TiO2 Nanoparticles with Semiconducting Polymers Containing a Photocleavable Anchor Group and Separation via Irradiation Afterward. *Macromolecular Chemistry and Physics* **2014**, *215* (7), 604–613. https://doi.org/10.1002/macp.201300759.

18 (18) Haynes, C. L.; McFarland, A. D.; Duyne, R. P. V. Surface-Enhanced Raman Spectroscopy. *Analytical Chemistry* **2005**, *77* (17), 338 A–346 A.

19 (19) Haynes, C. L.; Yonzon, C. R.; Zhang, X.; Van Duyne, R. P. Surface-Enhanced Raman Sensors: Early History and the Development of Sensors for Quantitative Biowarfare Agent and Glucose Detection. *J. Raman Spectrosc.* **2005**, *36* (6–7), 471–484. https://doi.org/10.1002/jrs.1376.

20 (20) Bantz, K. C.; Meyer, A. F.; Wittenberg, N. J.; Im, H.; Kurtuluş, Ö.; Lee, S. H.; Lindquist, N. C.; Oh, S.-H.; Haynes, C. L. Recent Progress in SERS Biosensing. *Phys Chem Chem Phys* **2011**, *13* (24), 11551–11567. https://doi.org/10.1039/c0cp01841d.

21 (21) Fenske, M. R.; Braun, W. G.; Wiegand, R. V.; Quiggle, D.; McCormick, R. H.; Rank, D. H. Raman Spectra of Hydrocarbons. *Anal. Chem.* **1947**, *19* (10), 700–765. https://doi.org/10.1021/ac60010a002.

22 (22) Chinnakkannu Vijayakumar, S.; Venkatakrishnan, K.; Tan, B. SERS Active Nanobiosensor Functionalized by Self-Assembled 3D Nickel Nanonetworks for Glutathione Detection. *ACS Appl. Mater. Interfaces* **2017**, *9* (6), 5077–5091. https://doi.org/10.1021/acsami.6b13576.

23 (23) Mayer, K. M.; Hafner, J. H. Localized Surface Plasmon Resonance Sensors. *Chem. Rev.* **2011**, *111* (6), 3828–3857. https://doi.org/10.1021/cr100313v.

24 (24) Le Ru, E. C.; Blackie, E.; Meyer, M.; Etchegoin, P. G. Surface Enhanced Raman Scattering Enhancement Factors: A Comprehensive Study. *J. Phys. Chem. C* **2007**, *111* (37), 13794–13803. https://doi.org/10.1021/jp0687908.

25 (25) Szlag, V. M.; Styles, M. J.; Madison, L. R.; Campos, A. R.; Wagh, B.; Sprouse, D.; Schatz, G. C.; Reineke, T. M.; Haynes, C. L. SERS Detection of Ricin B-Chain via N-Acetyl-Galactosamine Glycopolymers. *ACS Sens.* **2016**, *1* (7), 842–846. https://doi.org/10.1021/acssensors.6b00209.

26 (26) Duy, T. N.; Lam, P. K. S.; Shaw, G. R.; Connell, D. W. Toxicology and Risk Assessment of Freshwater Cyanobacterial (Blue-Green Algal) Toxins in Water. In *Reviews of Environmental Contamination and Toxicology*; Reviews of Environmental Contamination and Toxicology; Springer, New York, NY, 2000; pp 113–185. https://doi.org/10.1007/978-1-4757-6429-1_3.

27 (27) Milicevic, D.; Nesic, K.; Jaksic, S. Mycotoxin Contamination of the Food Supply Chain - Implications for One Health Programme. *Procedia Food Science* **2015**, *5*, 187–190. https://doi.org/10.1016/j.profoo.2015.09.053.

28 (28) Hussein, H. S.; Brasel, J. M. Toxicity, Metabolism, and Impact of Mycotoxins on Humans and Animals. *Toxicology* **2001**, *167* (2), 101–134. https://doi.org/10.1016/S0300-483X(01)00471-1.

29 (29) Eaton, D. L.; Groopman, J. D. *The Toxicology of*

Aflatoxins: Human Health, Veterinary, and Agricultural Significance; Elsevier, 2013.

30 (30) Center for Food Safety and Applied Nutrition. Chemical Contaminants, Metals, Natural Toxins & Pesticides - Guidance for Industry: Action Levels for Poisonous or Deleterious Substances in Human Food and Animal Feed http://www.fda.gov/Food/GuidanceRegulation/GuidanceDocumentsRegulatoryInformation/ChemicalContaminantsMetalsNaturalToxinsPesticides/ucm077969.htm#afla (accessed Jun 10, 2016).

31 (31) Stuart, D. A.; Yuen, J. M.; Shah, N.; Lyandres, O.; Yonzon, C. R.; Glucksberg, M. R.; Walsh, J. T.; Van Duyne, R. P. In Vivo Glucose Measurement by Surface-Enhanced Raman Spectroscopy. *Anal. Chem.* **2006**, *78* (20), 7211–7215. https://doi.org/10.1021/ac061238u.

32 (32) Kim, D.; Campos, A. R.; Datt, A.; Gao, Z.; Rycenga, M.; Burrows, N. D.; Greeneltch, N. G.; Mirkin, C. A.; Murphy, C. J.; Duyne, R. P. V.; et al. Microfluidic-SERS Devices for One Shot Limit-of-Detection. *Analyst* **2014**, *139* (13), 3227–3234. https://doi.org/10.1039/C4AN00357H.

33 (33) Campos, A. R.; Gao, Z.; Blaber, M. G.; Huang, R.; Schatz, G. C.; Van Duyne, R. P.; Haynes, C. L. Surface-Enhanced Raman Spectroscopy Detection of Ricin B Chain in Human Blood. *J. Phys. Chem. C* **2016**, *120* (37), 20961–20969. https://doi.org/10.1021/acs.jpcc.6b03027.

34 (34) Zaleski, S.; Clark, K. A.; Smith, M. M.; Eilert, J. Y.; Doty, M.; Van Duyne, R. P. Identification and Quantification of Intravenous Therapy Drugs Using Normal Raman Spectroscopy and Electrochemical Surface-Enhanced Raman Spectroscopy. *Anal. Chem.* **2017**, *89* (4), 2497–2504. https://doi.org/10.1021/acs.analchem.6b04636.

35 (35) Haynes, C. L.; Van Duyne, R. P. Nanosphere Lithography: A Versatile Nanofabrication Tool for Studies of Size-Dependent Nanoparticle Optics. *J. Phys. Chem. B* **2001**, *105* (24), 5599–5611. https://doi.org/10.1021/jp010657m.

36 (36) The Grain Inspection, Packers and Stockyards Administration. GIPSA's Role in Aflatoxin Testing https://www.gipsa.usda.gov/fgis/aflatoxin.aspx (accessed Jan 22, 2018).

37 (37) Piletska, E.; Karim, K.; Coker, R.; Piletsky, S. Development of the Custom Polymeric Materials Specific for Aflatoxin B1 and Ochratoxin A for Application with the ToxiQuant T1 Sensor Tool. *Journal of Chromatography A* **2010**, *1217* (16), 2543–2547. https://doi.org/10.1016/j.chroma.2009.11.091.

38 (38) Xu, X.; Smith, A. E.; Kirkland, S. E.; McCormick, C. L. Aqueous RAFT Synthesis of PH-Responsive Triblock Copolymer MPEO–PAPMA–PDPAEMA and Formation of Shell Cross-Linked Micelles†. *Macromolecules* **2008**, *41* (22), 8429–8435. https://doi.org/10.1021/ma801725w.

39 (39) Seuring, J.; Bayer, F. M.; Huber, K.; Agarwal, S. Upper Critical Solution Temperature of Poly(N-Acryloyl Glycinamide) in Water: A Concealed Property. *Macromolecules* **2012**, *45* (1), 374–384. https://doi.org/10.1021/ma202059t.

40 (40) Zhou, C.; Hillmyer, M. A.; Lodge, T. P. Micellization and Micellar Aggregation of Poly(Ethylene-Alt-Propylene)-b-Poly(Ethylene Oxide)-b-Poly(N-Isopropylacrylamide) Triblock Terpolymers in Water. *Macromolecules* **2011**, *44* (6), 1635–1641. https://doi.org/10.1021/ma102786q.

41 (41) Szlag, V. M.; Jung, S.; Rodriguez, R.; Bryson, S.; Bourgeois, M.; Schatz, G. C.; Reineke, T. M.; Haynes, C. L. Isothermal Titration Calorimetry for the Screening of Aflatoxin B1 Surface-Enhanced Raman Scattering Sensor Affinity Agents. *Analytical Chemistry* **In Preparation**.

42 (42) te Velde, G.; Bickelhaupt, F. M.; Baerends, E. J.; Fonseca Guerra, C.; van Gisbergen, S. J. A.; Snijders, J. G.; Ziegler, T. Chemistry with ADF. *J. Comput. Chem.* **2001**, *22* (9), 931–967. https://doi.org/10.1002/jcc.1056.

43 (43) Becke, A. D. Density-Functional Exchange-Energy Approximation with Correct Asymptotic Behavior. *Phys. Rev. A* **1988**, *38* (6), 3098–3100. https://doi.org/10.1103/PhysRevA.38.3098.

44 (44) Becke, A. D. A New Mixing of Hartree–Fock and Local Density-functional Theories. *The Journal of Chemical Physics* **1993**, *98* (2), 1372–1377. https://doi.org/10.1063/1.464304.

45 (45) R Core Team. *R: A Language and Environment for Statistical Computing*; R Foundation for Statistical Computing: Vienna, Austria, 2017.

46 (46) Lee, K.-M.; Herrman, T. J.; Bisrat, Y.; Murray, S. C. Feasibility of Surface-Enhanced Raman Spectroscopy for Rapid Detection of Aflatoxins in Maize. *J. Agric. Food Chem.* **2014**, *62* (19), 4466–4474. https://doi.org/10.1021/jf500854u.

47 (47) Wu, X.; Gao, S.; Wang, J.-S.; Wang, H.; Huang, Y.-W.; Zhao, Y. The Surface-Enhanced Raman Spectra of Aflatoxins: Spectral Analysis, Density Functional Theory Calculation, Detection and Differentiation. *Analyst* **2012**, *137* (18), 4226–4234. https://doi.org/10.1039/C2AN35378D.

48 (48) Zhao, Y.; Yang, Y.; Luo, Y.; Yang, X.; Li, M.; Song, Q. Double Detection of Mycotoxins Based on SERS Labels Embedded Ag@Au Core–Shell Nanoparticles. *ACS Appl. Mater. Interfaces* **2015**, *7* (39), 21780–21786. https://doi.org/10.1021/acsami.5b07804.

49 (49) Ko, J.; Lee, C.; Choo, J. Highly Sensitive SERS-Based Immunoassay of Aflatoxin B1 Using Silica-Encapsulated Hollow Gold Nanoparticles. *Journal of Hazardous Materials* **2015**, *285*, 11–17. https://doi.org/10.1016/j.jhazmat.2014.11.018.

50 (50) Duwez, A.-S.; Guillet, P.; Colard, C.; Gohy, J.-F.; Fustin, C.-A. Dithioesters and Trithiocarbonates as Anchoring Groups for the "Grafting-To" Approach. *Macromolecules* **2006**, *39* (8), 2729–2731. https://doi.org/10.1021/ma0602829.

51 (51) Fustin, C.-A.; Duwez, A.-S. Dithioesters and Trithiocarbonates Monolayers on Gold. *Journal of Electron Spectroscopy and Related Phenomena* **2009**, *172* (1–3), 104–106. https://doi.org/10.1016/j.elspec.2009.03.009.

52 (52) Slavin, S.; Soeriyadi, A. H.; Voorhaar, L.; Whittaker, M. R.; Becer, C. R.; Boyer, C.; Davis, T. P.; Haddleton, D. M. Adsorption Behaviour of Sulfur Containing Polymers to Gold Surfaces Using QCM-D. *Soft Matter* **2011**, *8* (1), 118–128. https://doi.org/10.1039/C1SM06410J.

53 (53) Jung, S.; Lodge, T. P.; Reineke, T. M. Complexation between DNA and Hydrophilic-Cationic Diblock Copolymers. *J. Phys. Chem. B* **2017**, *121* (10), 2230–2243. https://doi.org/10.1021/acs.jpcb.6b11408.

54 (54) Du, X.; Li, Y.; Xia, Y.-L.; Ai, S.-M.; Liang, J.; Sang, P.; Ji, X.-L.; Liu, S.-Q. Insights into Protein–Ligand Interactions: Mechanisms, Models, and Methods. *International Journal of Molecular Sciences* **2016**, *17* (2), 144. https://doi.org/10.3390/ijms17020144.

55 (55) Folkers, J. P.; Laibinis, P. E.; Whitesides, G. M. Self-Assembled Monolayers of Alkanethiols on Gold: Comparisons of Monolayers Containing Mixtures of Short- and Long-Chain Constituents with Methyl and Hydroxymethyl Terminal Groups. *Langmuir* **1992**, *8* (5), 1330–1341. https://doi.org/10.1021/la00041a015.

56 (56) Kamra, T.; Zhou, T.; Montelius, L.; Schnadt, J.; Ye, L. Implementation of Molecularly Imprinted Polymer Beads for Surface Enhanced Raman Detection. *Anal. Chem.* **2015**, *87* (10), 5056–5061. https://doi.org/10.1021/acs.analchem.5b00774.

57 (57) X. Zhang, F.; Han, L.; B. Israel, L.; G. Daras, J.; M. Maye, M.; Ly, N. K.; Zhong, C.-J. Colorimetric Detection of Thiol - Containing Amino Acids Using Gold Nanoparticles. *Analyst* **2002**, *127* (4), 462–465. https://doi.org/10.1039/B200007E.

58 (58)   Ebeling, B.; Vana, P. RAFT-Polymers with Single and Multiple Trithiocarbonate Groups as Uniform Gold-Nanoparticle Coatings. *Macromolecules* **2013**, *46* (12), 4862–4871. https://doi.org/10.1021/ma4008626.

59 (59)   Colthup, N. B.; Daly, L. H.; Wiberley, S. E. CHAPTER 12 - COMPOUNDS CONTAINING BORON, SILICON, PHOSPHORUS, SULFUR, OR HALOGEN. In *Introduction to Infrared and Raman Spectroscopy (Second Edition)*; Academic Press, 1975; pp 335–364. https://doi.org/10.1016/B978-0-12-182552-2.50015-2.

60 (60)   Blakey, I.; Schiller, T. L.; Merican, Z.; Fredericks, P. M. Interactions of Phenyldithioesters with Gold Nanoparticles (AuNPs): Implications for AuNP Functionalization and Molecular Barcoding of AuNP Assemblies. *Langmuir* **2010**, *26* (2), 692–701. https://doi.org/10.1021/la9023162.

61 (61)   Willcock, H.; K. O'Reilly, R. End Group Removal and Modification of RAFT Polymers. *Polymer Chemistry* **2010**, *1* (2), 149–157. https://doi.org/10.1039/B9PY00340A.

TOC for publishing:

Please do not adjust margins